Received: 27 December 2018 | Revised: 22 January 2019 | Accepted: 25 January 2019

DOI: 10.1002/maco.201810764

ARTICLE

Materials and Corrosion

Effect of seawater constituents on the performance of thermal spray aluminum in marine environments

Rosa G. Echaniz[1,2] | Shiladitya Paul[2,3] | Rob Thornton[2]

[1]National Structural Integrity Research Centre (NSIRC Ltd.), Cambridge, UK

[2]Department of Engineering, University of Leicester, Leicester, UK

[3]Materials Group, TWI Ltd, Cambridge, UK

Correspondence
Shiladitya Paul, TWI Ltd, Granta Park, Cambridge CB21 6AL, UK.
Email: shiladitya.paul@twi.co.uk

Funding information
Lloyd's Register Foundation; Engineering and Physical Sciences Research Council; UK Engineering and Physical Sciences Research Council, Grant/Award Number: EP/L016206/1

Abstract

Thermally sprayed coatings are often used to mitigate corrosion of offshore structures. They act as a physical barrier to the aggressive marine environment and as a sacrificial distributed anode for low carbon steel. In such environments, the severity of material degradation depends on many factors. The effect of temperature, exposure time or the presence of micro-organisms are the focus of many studies, for example, however, the effect of the different ions present in seawater remains largely unexplored. The chemical composition of the water changes considerably depending on the location; industrial, glacial, estuarine, and so forth. In addition, when thermal spray aluminum (TSA) protects steel in seawater, calcareous matter precipitates as a result of the cathodic polarization and subsequent localized increase in pH. Therefore, understanding how ions such as magnesium (II), calcium (II), or carbonates alter the coating properties in the marine environment is important. This paper reports the experimental work carried out with TSA-coated steel samples with defects to simulate mechanical damage or erosion of the coating. The combination of electrochemical tests and surface characterization provided evidence of the efficiency of the calcareous bilayer that forms on top of steel reducing the TSA degradation.

KEYWORDS

accelerated corrosion, calcareous deposits, cathodic protection, thermal spray aluminum

1 | INTRODUCTION

Low carbon steel is commonly used as a structural material for marine applications, despite its relatively poor corrosion resistance. Due to the high chloride levels present in marine environments, coupled with erosion and microbial effects, extensive material loss occurs in offshore platforms, pipelines, and ships. To mitigate the corrosion of steel in seawater, cathodic protection is used in the form of impressed current, sacrificial anodes and sacrificial coatings.[1]

Thermal spray aluminum (TSA) has been used for decades to prevent steel corrosion in subsea conditions, acting both as a physical barrier and as a sacrificial, anodic coating. TSA has been reported to provide protection for over 25 years, offering low maintenance and good performance at a low cost in places where inspection is not easy to perform.[2] It is well known that offshore corrosion depends on several parameters, such as dissolved oxygen content, the presence of microbial species, type and concentration of dissolved solids, and temperature among others. Laboratory investigations and

field studies have reported the ability of thermally sprayed coatings to effectively protect structures exposed to 5 wt% sodium chloride environments [3] as well as low calcium, chloride, and carbonate conditions.[4] The response of cathodically protected steel by the impressed current in a solution containing some of the ions present in seawater showed the formation of calcareous deposits on top of the steel.[5–7] However, studies on the influence of seawater chemistry and calcareous deposits formation on TSA with defects are lacking.

The chemical composition of seawater varies depending on the geographical location.[8–10] A clear example of this is the difference in salinity between oceanic water, brackish water, and fresh water. Among them, not only the total amount of salt content differ but also the proportion of the salts. While sodium chloride is the most common salt present in oceanic water, calcium carbonate is the most abundant salt present in fresh water. The presence and concentration of different compounds will affect the performance of TSA, since the corrosion products that deposit on top of the structures differ depending on them.

As the TSA is consumed to protect the steel, aluminum oxides, and hydroxides precipitate on top of it.[11] If the coating gets damaged due to erosion or microbiological effects, the steel is then directly exposed to the environment. In such cases, the cathodic reactions of oxygen reduction (Equation (1)) and hydrogen evolution (Equation (2)) predominantly occur on the steel surface.

$$O_2(g) + 2H_2O(l) + 4e^- \rightarrow 4OH^-(aq), \quad (1)$$

$$2H_2O(l) + 2e^- \rightarrow H_2(g) + 2OH^-(aq). \quad (2)$$

As a consequence, the pH increases locally next to the steel surface. In combination with the concentrations and solubility products of the different ions present in seawater, this causes the precipitation of calcareous deposits on cathodic sites (Equations (3) and (4))

$$Ca^{2+}(aq) + CO_3^{2-}(aq) \rightleftharpoons CaCO_3 \downarrow, \quad (3)$$

$$Mg^{2+}(aq) + 2OH^-(aq) \rightleftharpoons Mg(OH)_2 \downarrow. \quad (4)$$

Although one may expect calcium carbonate to precipitate first, based on local pH and solubility products, magnesium hydroxide is formed first due to the inhibiting effect of magnesium ions (Figure 1). Thus, calcareous deposits present a two-layered structure, with magnesium hydroxide in the inner layer and calcium carbonate in the outer layer.[12] From these initial considerations, it is evident that the precipitating species, along with the precipitation kinetics, play an important role in the performance of TSA. In addition, understanding the effect of different ions on the precipitation of deposits may allow for more accurate modeling of TSA performance in different environments. Thus, the aim of this study was to evaluate the performance of TSA with defects in different solutions containing the key ions present in seawater.

In the present study, long-term laboratory tests (90 days) were performed to establish the behavior of TSA, over time, in different seawater chemistry solutions. From the electrochemical data, the performance of the TSA, after the failure of the coating, has been verified with corrosion rates lower than 20 μm/year after 90 days of exposure to different solutions. Different deposits were identified through surface characterization, dependent on the solution, such as brucite (magnesium hydroxide), calcite and aragonite (calcium carbonate).

2 | EXPERIMENTAL

2.1 | Materials

Low carbon steel (S355) coupons were used as substrates for the coating (40 × 40 × 6 mm), with nominal compositions shown in Table 1. Before the thermal spray process, angular alumina (NK36 type; 0.250–0.297 mm) and pressure were used for the grit blasting of the steel substrates, to achieve standard cleanliness of SA 2.5.

These substrates were coated with commercially pure aluminum (1050 alloy, 99.5% aluminum) by twin wire arc spray (TWAS) with a 528 gun (Metallisation Ltd, Dudley, UK) using parameters shown in Table 2. TSA coatings present a rough surface (*Ra*, 17.75 μm) in comparison with the steel substrate (*Ra*, 2.35 μm), and 5–10% interlamellar porosity.

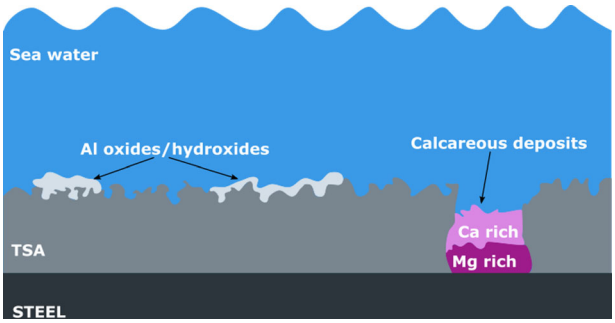

FIGURE 1 Schematic diagram of thermal spray aluminum performance in sea water. Al oxides/hydroxides precipitate on top of the coating, whereas calcareous deposits appear if steel is exposed to the sea water

TABLE 1 Nominal composition of S355 steel substrates

Elements	C	Mn	Si	P	S	Cr	Ni	Cu	Al	Mo
Wt%	0.150	1.350	0.030	0.016	0.005	0.080	0.060	0.170	0.035	0.014

TABLE 2 Thermal spray process parameters

Wire diameter (mm)	Wire feed rate (m/min)	Spray distance (mm)	Increment step (mm)	Traverse speed (m/s)	Voltage (V)	Nominal thickness (μm)
2.3	5.0	95.0	10.0	0.45	33.0	200–300

Once the coating was sprlayed onto the substrate, samples were prepared for the electrochemical tests. Circular holidays (artificial defects) were machined with a flat drill bit at the center of each sample (ø 10 mm, 0.8 mm depth, covering 5% of sample surface area) to simulate coating failure. The electrical connection was created by a threaded rod on the sample's side, and all sides of the sample except for the TSA-coated one were covered with a Type 45 stopping off lacquer (MacDermid plc, Birmingham, UK).

For examination of cross-sections, samples were cut with a vertical abrasive cutting saw Buehler Abrasmatic 300 (Buehler, Lake Bluff, Illinois, USA) and cold mounted with Clarocit resin. Grinding of the surface was carried out with a grinding wheel ATM Saphir 350l (ATM, Mammelzen, Germany) and silicon carbide abrasive papers going from P120 to P2500. Finally, polishing was performed with a polishing wheel Buehler Metaserv 250 (Buehler, Lake Bluff, IL) by successively using 3 and 1 μm diamond paste.

All solutions used for electrochemical tests are shown in Table 3, prepared from analytical grade chemical reagents (Thermo Fisher Scientific, Waltham, MA) and deionized water (13 MΩ cm). Sodium chloride was added to maintain a constant ionic strength of the solutions. The pH was adjusted to 8.2 by controlled addition of sodium hydroxide (1% v/v). To compare results, commercial synthetic seawater (ASTM D1141, ReAgent, Runcorn, UK) was used.

2.2 | Electrochemical tests

The instrument used to carry out the tests was a Biologic VMP3 potentiostat/galvanostat (Bio-Logic Science Instruments, Seyssinet-Pariset, France), and the software used for analysis was EC-Lab (Bio-Logic Science Instruments), provided by the same company as the equipment. All electrochemical measurements were carried out using a three-electrode configuration system and using the solutions described in Table 3 as electrolytes. Individual cells open to air were used for each solution, with a silver/silver chloride (potassium chloride sat.) reference electrode (RE), platinum/titanium wire counter or auxiliary electrode (AE) and TSA coated steel sample with the holiday as the static working electrode (WE). Long term tests were 90 days in duration, with pH and temperature monitored daily. In addition, cells with only the solutions (no electrodes) were prepared to study the pH changes. The size of these cells matched the ones containing the electrodes, with the same volume of solution and, therefore, the same surface area of liquid exposed to the atmosphere. All cells were kept in a water bath to expose the specimens at a constant ambient temperature of 26°C ± 1°C (Figure 2).

Electrochemical monitoring was carried out by using: (a) open circuit potential (OCP) and (b) linear polarization resistance (LPR) measurements once every 24 hr. From the LPR data, the corrosion rates (CR) were obtained using Equation (5), where I_{corr} is the corrosion current (A), K is a constant, EW corresponds to the equivalent weight of the corroding metal (mass/number of electrons involved), d corresponds to the density of the corroding metal (g/cm^3) and A is the area exposed to the electrolyte solution (cm^2).

$$\mathrm{CR(mm/year)} = \frac{I_{corr} \bullet K \bullet \mathrm{EW}}{d \bullet A}. \quad (5)$$

TABLE 3 Chemical composition of electrolytes and ionic strength in mol/L

Electrolyte	$MgCl_2$	$CaCl_2$	$NaHCO_3$	Na_2SO_4	KCl	KBr	Ionic strength
ASTM D1141	0.055	0.010	0.002	0.029	0.009	0.0008	0.703
S1	0.055	–	0.002	–	–	–	0.695
S2	–	0.010	0.002	–	–	–	0.630
S3	0.055	0.010	0.002	–	–	–	0.704

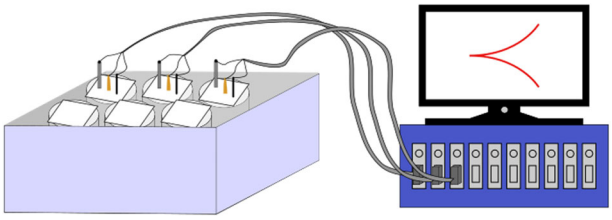

FIGURE 2 Schematic diagram of experimental set up. Bath with six cells on the left side, three with electrodes immersed and connected to the potentiostat, and three with no electrodes to monitor pH changes of solution

LPR measurements were performed in the range of ±10 mV from the corrosion potential (E_{corr}), at 10 mV/min. Polarization curves performed on different solutions were carried out within a ±250 mV range from E_{corr} and a 50 mV/min scan rate.

2.3 | Characterization

Surface topography and chemical composition of the samples were evaluated after exposure to different solutions. Corrosion products formed on the surface of the specimens were characterized by scanning electron microscopy and energy dispersive X-ray spectroscopy (SEM/EDX), and X-ray diffraction (XRD).

Topographical and chemical analyses were performed using an EVO LS15 SEM (Zeiss, Obekochen, Germany) using 20 kV voltage, 4.5 spot size, 8.5 mm working distance, and backscattered electron detector. Crystallographic measurements were performed with a Bruker D8-Advanced (Bruker, Billerica, MA) using Cu-Kα radiation and collecting data over the 2θ range of 0° to 80°.

3 | RESULTS AND DISCUSSION

3.1 | Deposits characterization

3.1.1 | Visual inspection

After 90 days of exposure, corrosion deposits were formed both on top of the TSA coating and the holiday region. Figure 3 shows the appearance of the samples before and after the tests. On top of the TSA coating, a similar type of deposits are observed independently of the solution they were exposed to. On top of steel, no rust is observed with the naked eye, although different types of deposits were formed. Deposits formed on S1 and S3 present a white appearance, while deposits formed on S2 present a translucent look. Moreover, calcareous deposits accumulate in all cases on the edge of the holiday due to a greater polarization within this region.

3.1.2 | Microstructural characterization

Surface characterization of the samples was performed after exposure to confirm the composition of the calcareous deposits. Figure 4 shows SEM images after corrosion as the top view from the holiday region of the samples. From these, three types of structures can be distinguished; disc clusters, cubes, and elongated crystals. Disc clusters (•) are present in samples exposed to solutions containing magnesium ions, S1 and S3. Cubic structures (■) are present exclusively in solution S2, and elongated crystals (▲) are present in solution S3 combined with the disc clusters.

Figure 5 shows the cross-section from the sample exposed to solution 3 exhibiting a bilayer structure of the deposits. The darker inner layer corresponds to the more compact disc clusters structures, whereas the lighter in color outer layer corresponds to the elongated crystals.

EDX analysis performed locally on each morphology reveals their chemical composition (Figure 6). Disc clusters consist of magnesium and oxygen elements mainly, while cubes and elongated crystals consist of calcium, carbon, and oxygen.

The crystal structure of the deposits formed over 90 days of exposure to the different solutions was confirmed by XRD patterns (Figure 7). Brucite (magnesium hydroxide) was identified in solution S1 with the main diffraction lines at 2θ ~19°, 38°, and 51°, corresponding to the disc clusters. In solution S2, calcite (calcium carbonate) was identified with its characteristic peak at ~30°, associated then to the cubic structures. Regarding solution S3, aragonite (calcium carbonate) was found as the elongated crystals presenting several peaks between 25° and 55°, in combination with brucite. However, the calcite peak

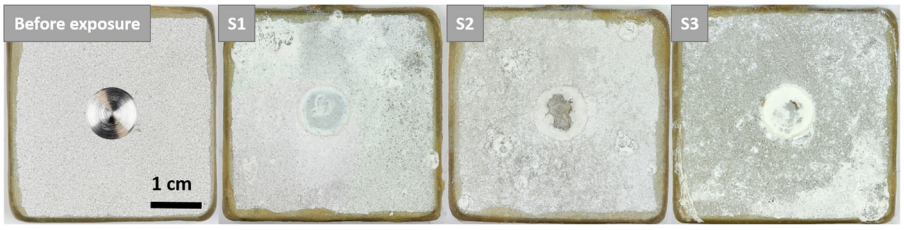

FIGURE 3 Images of thermal spray aluminum samples with defects obtained before and after 90 days of exposure to solutions S1, S2, and S3

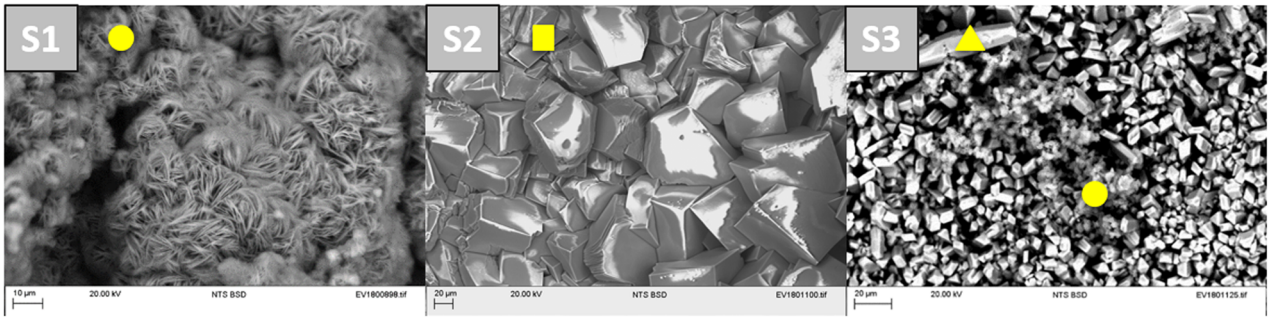

FIGURE 4 SEM images from defect area of thermal spray aluminum samples after 90 days exposure to solutions S1, S2, and S3

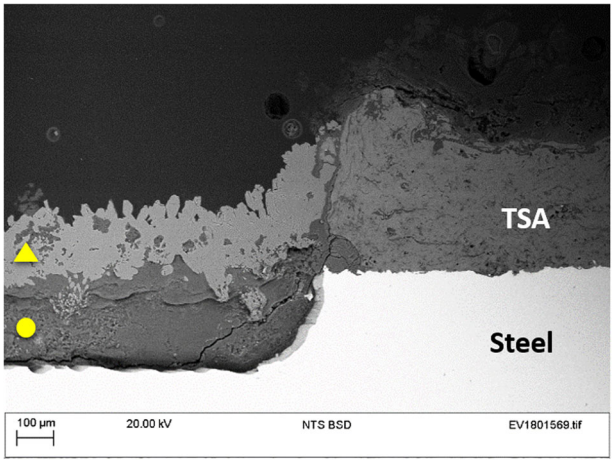

FIGURE 5 Cross section of interface between thermal spray aluminum and defect area on sample exposed to S3 for 90 days

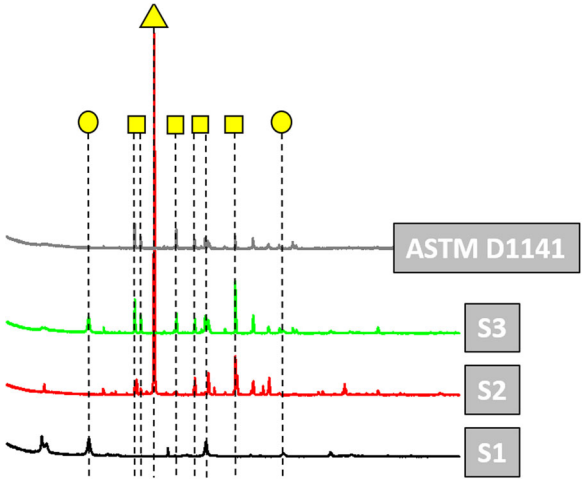

FIGURE 7 X-ray powder diffraction analysis of deposits from defect area of thermal spray aluminum samples exposed to solutions S1, S2, S3, and artificial seawater (ASTM D1141) for 90 days

at ~30° was not found. Comparisons with the scales formed due to exposure to artificial seawater (ASTM D1141) reveal brucite and aragonite, but no calcite in contrast to the sample exposed to solution S2.[13] Here, the inhibiting effect of magnesium ions is shown once again as calcite is not identified.

Calcareous deposits described appear only on the defect areas where the steel substrate is exposed. On top of the aluminum coating, aluminum amorphous oxides/hydroxides are formed blocking the pores of the TSA. SEM/EDX analysis on the coating reveals undistinguishable results among all samples, including, the one exposed to artificial seawater.

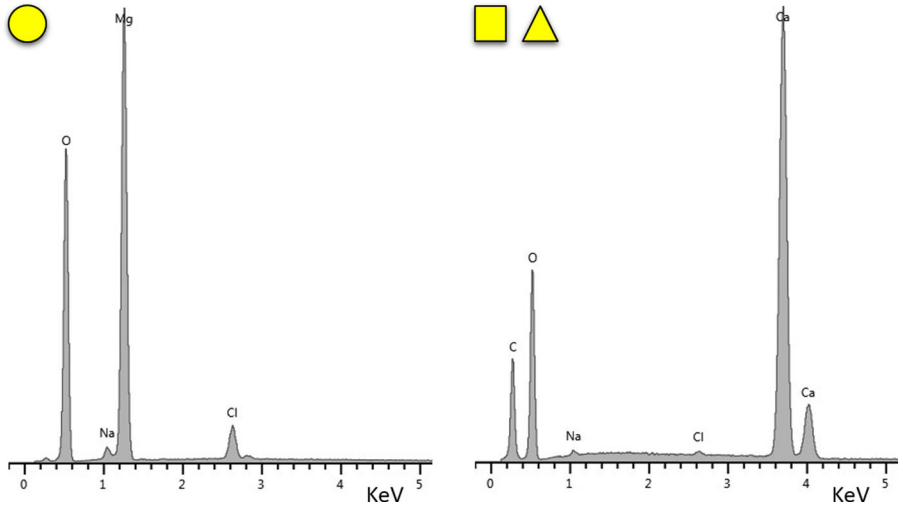

FIGURE 6 X-ray powder diffraction analysis of scales formed on defect areas of thermal spray aluminum samples after 90 days exposure to solutions S1, S2, and S3

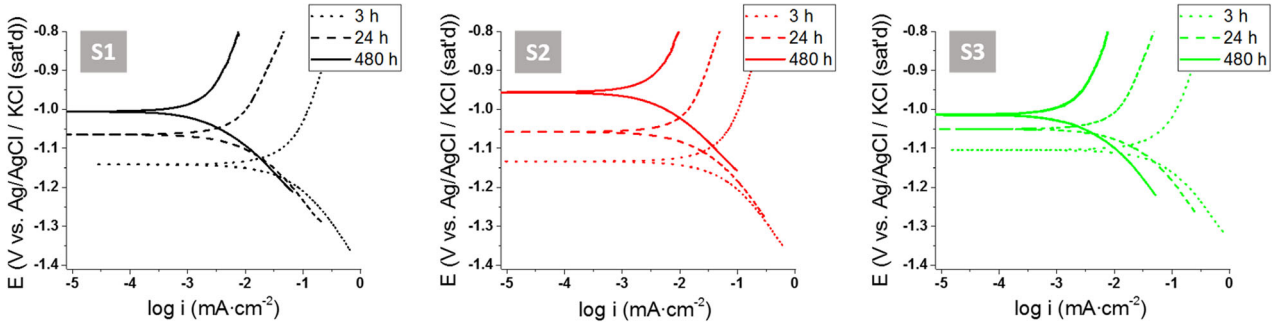

FIGURE 8 Polarization curves of thermal spray aluminum with defects over time with three different solutions as electrolytes (S1, S2, and S3)

3.2 | Electrochemical measurements

3.2.1 | Polarization curves

Polarization curves of TSA samples with defects were performed after 3, 24, and 480 hr of immersion in solutions S1, S2, and S3 (Figure 8). As the time of exposure to each solution increases, the corrosion current density decreases and the corrosion potential shifts toward less negative values. This is attributed to the formation of corrosion deposits on top of the samples.

The exposure of the TSA coating and the steel substrate within the same sample results in a mixed potential for the sample. For this system, the cathodic current would be dominated by the reduction of dissolved oxygen on the exposed steel surface and the dissolution of aluminum would contribute predominantly to the anodic current.

On the cathode, calcareous deposits accumulate acting as a physical barrier for oxygen diffusion. The calcareous deposits are also poor electron conductors, hence decreasing the current density and requiring less sacrificial anode consumption. Nucleation, growth, and structure of the scales will vary depending on the ions present in each solution.[5–7,14]

In S1, magnesium ions lead to the formation of a sol–gel like a homogeneous porous layer of brucite (magnesium hydroxide). In S2, the presence of calcium ions without magnesium ions lead to the formation of single crystals of calcium carbonate resulting in a heterogeneous layer of calcite. Finally, in S3, where both magnesium and calcium ions were present, there was a bilayer scale formation with brucite in the inner layer on top of the steel substrate and calcium carbonate as aragonite on the outside layer.

The transformation of the calcium carbonate precipitate between S2 and S3 is due to the presence of magnesium ions in S3. These ions incorporate within the calcite crystal structure as it grows to form an Mg-calcite compound which is more soluble.[15] Therefore, calcite formation in the presence of magnesium ions in solution is inhibited and only aragonite is formed under these conditions. The porosity of the deposits decreases as their thickness increases on top of the steel substrate (the cathodic area of the samples).

In all cases, the anodic branch is inhibited over time. As the aluminum dissolves to polarize the steel, aluminum oxides/hydroxides precipitate on top of the TSA coating passivating its surface. The cathodic branch evolution differs among the three solutions. Depending on the type of scales being formed on top of the cathode, the reaction of oxygen/water reduction changes. According to the deposits previously described, S1 forms a homogeneous porous layer of brucite which reduces the cathodic current density slightly. S2 forms a heterogeneous layer which cannot block the entire surface of the cathode resulting in the cathodic reaction being unaltered. Finally, S3 presents a mixed structure of brucite and aragonite providing better coverage of the cathode which inhibits the water/oxygen reaction more effectively.

3.2.2 | Long term tests

Long-term corrosion performance of TSA coating with defects was monitored over 90 days by LPR to obtain the corrosion rates. The graph showing the OCP values in Figure 9 presents two regions; one where potential drops drastically and then increases to reach a more stable value, and the other where small potential changes occur progressively over time. The first region occurs over the first 72 hr of the tests. These initial changes are attributed to the formation of the first calcareous deposits on top of the steel, the dissolution of the air-formed film on top of the TSA coating and/or the formation of aqueous-formed films of aluminum oxides/hydroxides. By the end of the tests, OCP values for all samples are within −0.90 and −1.12 V (vs. silver/silver chloride).

Corrosion rates were calculated to evaluate the TSA performance over time and quantify the corrosivity of the solutions. One could argue that the use of LPR for measuring corrosion rates of TSA with a defect may not be strictly valid; however, the data gives some indication

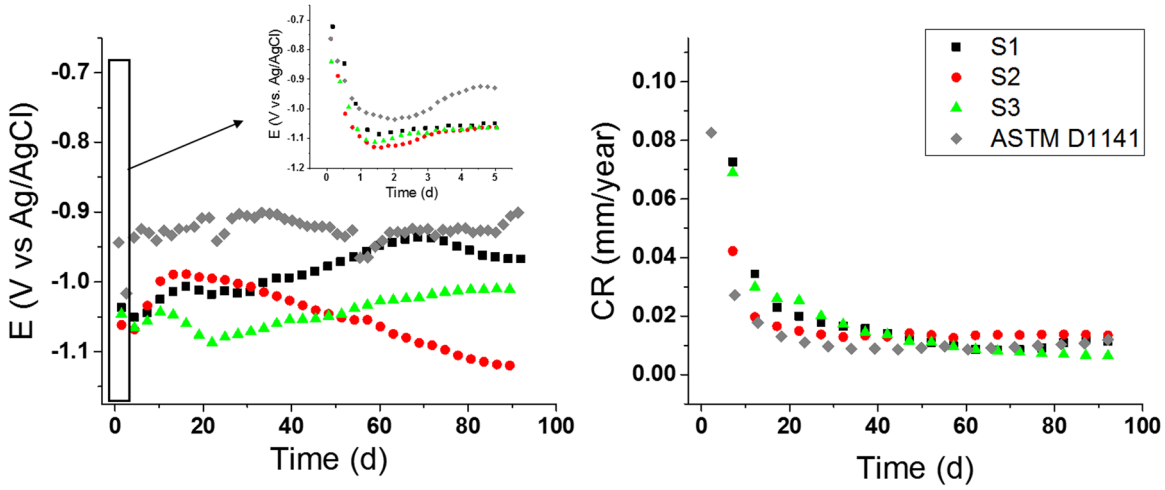

FIGURE 9 Open circuit potential and corrosion rate obtained over 90 days by exposure of thermal spray aluminum with defects to four solutions: S1, S2, S3, and artificial seawater (ASTM D1141)

regarding the performance of TSA containing defects. During the initial stage of exposure, the steel surface is bare and this is expected to give mixed potential and the anodic and cathodic currents cannot be separated. However, as the deposits are formed on the steel surface over time one may tend to get more useful information using LPR as the anodic and cathodic reactions are likely to occur on the TSA surface. As a result, the corrosion rates decrease over time, from 80 μm/year at the beginning of the test to less than 20 μm/year after 90 days of exposure, showing that TSA can protect the underlying steel even after a coating defect exposing 5% of steel is introduced before exposure.

Values obtained in artificial seawater over the same period of time are presented here as well. The behavior of TSA in artificial seawater has been previously reported looking at different environmental parameters such as temperature, pH or position within the offshore structure (atmospheric, splash, tidal, or submerged).[16–18] Comparing these with data obtained in the present studies, corrosion rates at the end of the test are of the same order of magnitude. This is despite the modification of the chemical composition of the electrolyte and more negative potential values being recorded for solutions S1, S2, and S3.

3.3 | pH monitoring

Over the course of the long-term experiments, pH was continuously monitored. Seawater pH is between 7.8 and 8.3 at room temperature. Fluctuations between these values depend on the carbon dioxide dissolution from the atmosphere, acting as a buffer according to Equation (6), and salts content.

$$CO_2(aq) + H_2O \rightleftharpoons H_2CO_3 \rightleftharpoons H^+ + HCO_3^- \rightleftharpoons CO_3^{2-} + 2H^+. \quad (6)$$

Figure 10 shows the experimental data obtained for the three solutions tested with and without a TSA sample

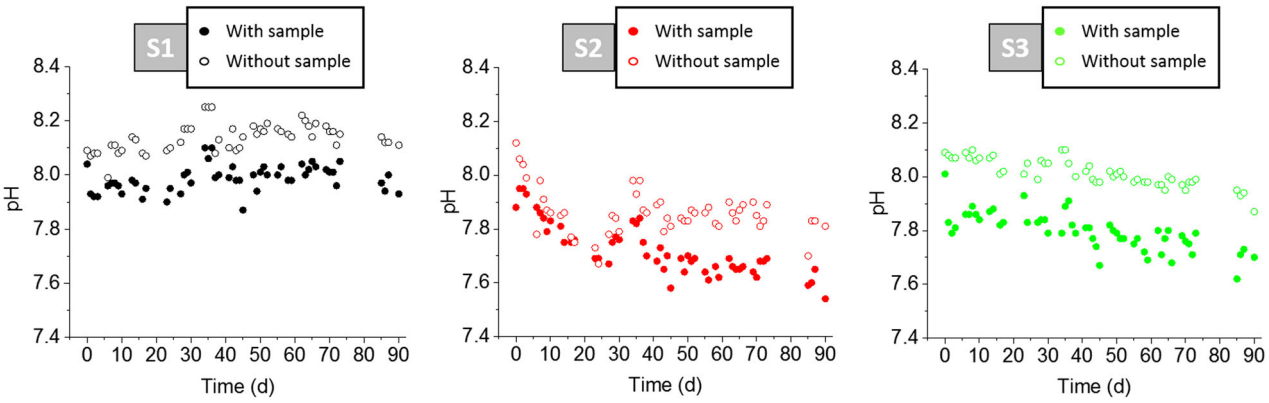

FIGURE 10 pH values of electrolyte solutions (S1, S2, and S3) recorded over 90 days with and without a sample being immersed in solution

immersed. From these graphs, solutions S1 and S3 present similar trends. Solutions containing the sample show lower values of pH through the whole duration of the experiment in both cases. For solutions where no samples have been immersed, carbon dioxide dissolution from air and water evaporation/addition are the cause of the variations observed. When samples are present, anodic reactions of aluminum dissolving into solution, and hydrolyzing can acidify the environment following Equations (7) and (8).[11] In addition, cathodic reactions provide hydroxide ions that promote precipitation of brucite in S1 and brucite and aragonite in S3.

$$Al(s) \longrightarrow Al^{3+} + 3e^{-}, \tag{7}$$

$$Al^{3+} + 3H_2O \rightleftharpoons Al(OH)_3 + 3H^{+}. \tag{8}$$

However, pH values in solution S2 presented a different trend where the presence of the sample had no effect on the initial value. Here, the metal dissolution on the anodic sites competes with the formation of the calcareous deposits of calcite due to the absence of magnesium ions. Nucleation of calcite is a slow process, which would correspond to the initial part of the S2 graph. Once the crystals enter the growing phase, postnucleation, they grow faster on top of the cathode area than in bulk. The localized increase of OH^- from the cathodic reaction leads to an increase in the concentration of carbonates as well (Equation (9)).

$$OH^- + HCO_3^- \rightleftharpoons CO_3^{2-} + H_2O. \tag{9}$$

As a result, calcite crystals formation is enhanced on top of the cathode and the pH of the solution containing the sample decreases compared to the one without it.

4 | SUMMARY AND CONCLUSIONS

The work carried out shows that TSA is able to protect steel in various environments even in presence of defects. Artificially damaged TSA coatings were exposed to solutions containing different ions present in seawater, continuously monitored by electrochemical techniques and their surfaces subsequently characterized. From polarization curves, it was shown that the formation of deposits resulted in decreasing current densities over time. As scales form, they act as a physical barrier and offer protection against further corrosion. Thicker and more compact deposits provide better coverage and, therefore, protect the steel more efficiently. The use of electrochemical techniques such as OCP and LPR over the test duration provided data describing the evolution of the system. Potential changes over the first few days showed the polarization of the exposed steel by the TSA coating. During these initial stages, air-formed oxides from the coating dissolved and new oxides/hydroxides of aluminum formed. By the end of the tests, OCP values were within the cathodic protection region for steel and corrosion rates were estimated to be <20 μm/year.

Surface characterization of samples was performed after 90 days of corrosion in different solutions. Aluminum oxides/hydroxides deposited on top of the coating and blocked its porosity independently of the solutions samples were exposed to. However, in the defect areas the calcareous deposits formed differed among solutions: (a) in the presence of magnesium ions only a homogeneous layer of brucite is formed; (b) in presence of calcium ions only a heterogeneous layer of calcite is formed and; (c) when both magnesium and calcium are present a bilayer is formed with brucite in the inner layer and aragonite in the outer layer. The bilayer is more dense, providing better coverage and more efficient protection of the steel substrate underneath. Therefore, the protection offered by calcareous deposits would be expected to vary depending on the environment where offshore structures might be located.

Overall, the data collected from electrochemical methods and surface characterization have provided useful information in view of the application of cathodic protection of TSA for steel in different environments after coating damage occurs. It shows how testing coatings in solutions consisting of a range of ions and concentrations can be used to predict their response to unknown environments. This could be achieved by using tools such as a design of experiments approach, which could be a future output.

ACKNOWLEDGMENTS

The authors gratefully acknowledge financial support from the Centre for Doctoral Training in Innovative Metal Processing (IMPaCT) funded by the UK Engineering and Physical Sciences Research Council (EPSRC), grant reference EP/L016206/1. This publication was made possible by the sponsorship and support of Lloyd's Register Foundation, a charitable foundation helping to protect life and property by supporting engineering-related education, public engagement and the application of research. The work was enabled through, and undertaken at, the National Structural Integrity Research Centre (NSIRC), a postgraduate engineering facility for industry-led research into structural integrity established

and managed by TWI through a network of both national andinternational Universities. Raw data relating to this study is available at https://doi.org/10.25392/leicester.data.c.4390133.

ORCID

Shiladitya Paul http://orcid.org/0000-0002-8423-313X

REFERENCES

[1] W. H. Hartt, *Corrosion* **2012**, *68*, 1063.
[2] K. P. Fischer, W. H. Thomason, T. Rosbrook, J. Murali, *Mater. Perform.* **1995**, *34*, 27.
[3] V. R. S. Sá Brito, I. N. Bastos, H. R. M. Costa, *Mater. Des.* **2012**, *41*, 282.
[4] H.-S. Lee, J. Singh, M. Ismail, C. Bhattacharya, *Metals* **2016**, *6*, 55.
[5] C. Deslouis, D. Festy, O. Gil, G. Rius, S. Touzain, B. Tribollet, *Electrochim. Acta* **1998**, *43*, 1891.
[6] C. Deslouis, D. Festy, O. Gil, V. Maillot, S. Touzain, B. Tribollet, *Electrochim. Acta* **2000**, *45*, 1837.
[7] C. Barchiche, C. Deslouis, D. Festy, O. Gil, P. Refait, S. Touzain, B. Tribollet, *Electrochim. Acta* **2003**, *48*, 1645.
[8] J. Safarov, S. Berndt, F. J. Millero, R. Feistel, A. Heintz, E. P. Hassel, *Deep Sea Res. I* **2013**, *78*, 95.
[9] W. S. Moore, *Mar. Chem.* **1999**, *65*, 111.
[10] R. J. Gibbs, *Science* **1970**, *170*, 1088.
[11] E. Deltombe, M. Pourbaix, *Corrosion* **1958**, *14*, 496.
[12] W. H. Hartt, C. H. Culberson, S. W. Smith, *Corrosion* **1984**, *40*, 609.
[13] C. Rousseau, F. Baraud, L. Leleyter, M. Jeannin, O. Gil, *Corros. Sci.* **2010**, *52*, 2206.
[14] C. Barchiche, C. Deslouis, O. Gil, P. Refait, B. Tribollet, *Electrochim. Acta* **2004**, *49*, 2833.
[15] R. A. Berner, *Geochim. Cosmochim. Acta* **1975**, *39*, 489.
[16] S. Kuroda, J. Kawakita, M. Takemoto, *Corrosion* **2006**, *62*, 635.
[17] N. Ce, S. Paul, *Coatings* **2017**, *7*, 52.
[18] B.-R. Hou, J. Zhang, J.-Z. Duan, Y. Li, J.-L. Zhang, *Corros. Eng. Sci. Technol.* **2003**, *38*, 157.

How to cite this article: Echaniz RG, Paul S, Thornton R. Effect of seawater constituents on the performance of thermal spray aluminum in marine environments. *Materials and Corrosion*. 2019;70: 996–1004. https://doi.org/10.1002/maco.201810764